lubricants

MDPI

Article

Tribological, Oxidation and Thermal Analysis of Advanced Microwave—Hydrothermal Synthesised $Ti_3C_2T_x$ MXene as Additives in Outboard Engine Oil

Haizum Aimi Zaharin [1,*], Mariyam Jameelah Ghazali [1,*], Mohammad Khalid [2,3,4,5,*], Thachnatharen Nagarajan [6], Wong Weng Pin [2], Farah Ezzah [7], Ong Gerard [8], Rashmi Walvekar [9] and Abdul Khaliq Rasheed [10]

1 Department of Mechanical and Manufacturing Engineering, Faculty of Engineering and Built Environment, Universiti Kebangsaan Malaysia, Bangi 43600, Malaysia
2 Graphene and Advanced 2D Materials Research Group (GAMRG), School of Engineering and Technology, Sunway University, Petaling Jaya 47500, Malaysia
3 Sunway Materials Smart Science and Engineering (SMS2E) Research Cluster, Sunway University, Petaling Jaya 47500, Malaysia
4 School of Applied and Life Sciences, Uttaranchal University, Dehradun 248007, India
5 Division of Research and Development, Lovely Professional University, Phagwara 144411, India
6 Faculty of Defence Science and Technology, National Defence University of Malaysia, Kuala Lumpur 57000, Malaysia
7 Department of Chemical and Environmental Engineering, Malaysia-Japan International Institute of Technology (MJIIT), Universiti Teknologi Malaysia, Jalan Sultan Yahya Petra, Kuala Lumpur 54100, Malaysia; farahezzah.fea@gmail.com
8 Centre for Ionics University of Malaya, Department of Physics, Faculty of Science, Universiti Malaya, Kuala Lumpur 50603, Malaysia
9 Department Chemical Engineering, School of Energy and Chemical Engineering, Xiamen University Malaysia, Bandar Sunsuria, Sepang 43900, Malaysia; rashmi.walvekar@xmu.edu.my
10 Department of New Energy Science and Engineering, School of Energy and Chemical Engineering, Ximen University Malaysia (XMUM), Sepang 43900, Malaysia; abdulkhaliq.rasheed@xmu.edu.my
* Correspondence: p100279@siswa.ukm.edu.my (H.A.Z.); mariyam@ukm.edu.my (M.J.G.); khalids@sunway.edu.my (M.K.)

check for updates

Citation: Zaharin, H.A.; Ghazali, M.J.; Khalid, M.; Nagarajan, T.; Pin, W.W.; Ezzah, F.; Gerard, O.; Walvekar, R.; Rasheed, A.K. Tribological, Oxidation and Thermal Analysis of Advanced Microwave—Hydrothermal Synthesised $Ti_3C_2T_x$ MXene as Additives in Outboard Engine Oil. *Lubricants* **2023**, *11*, 264. https://doi.org/10.3390/lubricants11060264

Received: 30 May 2023
Revised: 14 June 2023
Accepted: 15 June 2023
Published: 16 June 2023

Abstract: In today's fast, globalised world, lubrication has become essential in enhancing engine efficiency, including in the marine sector. While the number of fishing vessels increased, so did the environmental pollution issues, due to inefficient engines. An outboard engine oil's tribological, oxidation and thermal conductivity behaviour play a crucial role in improving the quality of an outboard engine's life. In this research, $Ti_3C_2T_x$ MXene nanoparticles with different interlayer spacing were synthesised via an advanced microwave–hydrothermal approach. Later, the nanoparticles were dispersed in TC-W outboard engine oil to formulate the $Ti_3C_2T_x$ MXene nanolubricant with different concentrations. The results show that nanolubricant with a 0.01 wt.% $Ti_3C_2T_x$ MXene concentration with higher interlayer spacing reduced the coefficient of friction, and the average wear scar diameter by 14.5% and 6.3%, respectively, compared to the base oil. Furthermore, the nanolubricant with a 0.01 wt.% concentration of the $Ti_3C_2T_x$ MXene nanoparticle showed an improvement of 54.8% in oxidation induction time compared to the base oil. In addition, MXene nanolubricant established a more than 50% improvement in thermal conductivity compared to the base oil.

Keywords: MXene; tribology; nanolubricant; oxidation; thermal conductivity

1. Introduction

The rapidly expanding numbers of engine-powered fishing vessels, seafood industries and sea transport in international trade have resulted in a rise in the use of marine engines, which reward the world with beneficial effects on economic growth [1]. However, the

offering does not come empty-handed, and there is a high price we have to pay. Human health, aquatic life, and the air and marine environment have all been compromised due to the poisonous emissions from inefficient marine engines and lubricants [1–4]. Therefore, improved marine engine oil is extremely important for enhancing engine performance and efficiency. Enhancing marine lubrication is expected to reduce wear and friction, extend the life of the mechanical components, increase fuel efficiency, and lower emissions. Furthermore, improved lubrication protects health and the environment, especially for populations living near ports and coasts, including aquatic species, in agreement with the United Nations Sustainable Development Goals (SDGs); in particular, for SDG 14, which is focused on "Life Below Water," it is crucial to explore innovative solutions that can mitigate marine pollution and promote sustainable practices, as well as SDG 13, climate action, SDG 14, underwater life and SDG 15, life on land [5].

Researchers have shifted their focus onto harnessing nanomaterials to enhance traditional lubricants and optimise engine performance, due to the rapid growth of nanotechnology. It is feasible to improve lubrication, boost fuel efficiency, and extend engine life by introducing nanotechnology nanoparticles into the outboard engine oil and ultimately contribute to reducing marine pollution [6,7]. Nanolubricants are specially engineered at the nanoscale, allowing them to offer enhanced lubricating properties compared to conventional lubricants. These nanoscale additives possess unique characteristics that minimise friction and wear between engine components [8–10]. By reducing friction, nanolubricants help optimise the engine's mechanical efficiency, improving fuel economy and reducing emissions. In addition to their superior lubricating properties, nanolubricants exhibit enhanced thermal stability. The nanoscale structure of these lubricants enables better heat dissipation, reducing the risk of thermal degradation and maintaining optimal operating temperatures within the engine [11,12]. This improved thermal stability translates to more efficient engine performance and longevity.

Nanotechnology is the manipulation and control of materials at the nanoscale level, which is generally between 1 and 100 nanometres. Materials have distinctive characteristics at this size that differ from their bulk counterparts. The capacity to manufacture nanoparticles with specific properties and functions has opened up new possibilities for improving lubricants in various applications [13]. The incorporation of nanoparticles into engine oil has various prospective benefits. Firstly, nanoparticles can minimise friction between moving engine parts by generating a protective coating that lowers metal-to-metal contact, thus reducing wear and tear [14,15]. Additionally, these nanoparticles can improve thermal conductivity, allowing for improved heat dissipation and lower operating temperatures. This characteristic is especially important for outboard engines used in harsh maritime conditions. Furthermore, the unique physicochemical features of nanoparticles can improve the engine oil's detergency and dispersibility, boosting its capacity to remove and suspend pollutants [16].

Furthermore, emerging research suggests that incorporating 2D MXene additives into marine engine oils holds great potential in addressing tribological problems [17] and significantly reducing pollution. MXenes are two-dimensional (2D) materials with layered transition metal carbides, nitrides, or carbonitrides. These 2D materials are typically prepared by etching initial materials known as MAX phase, represented by the generalised formula $M_{n+1}AX_n$. Here, "M" stands for the transition metals, "A" is an element from group 12 to 16 of the periodic table, "X" can be either carbon (C) or nitrogen (N), while "n" in this formula can range from 1 to 3 [18–21]. $Ti_3C_2T_x$ MXene, in particular, has received a lot of interest in recent years due to its exceptional features, including strong electrical conductivity, thermal stability, and excellent mechanical strength [22,23]. These properties make it an intriguing choice for adding to engine oil in order to improve lubrication and reduce engine friction. Dispersing $Ti_3C_2T_x$ MXene nanoparticles into engine oil has many potential advantages [24]. These nanoparticles can build a strong protective coating on the engine surfaces, minimising friction and wear between moving parts. The $Ti_3C_2T_x$ MXene's peculiar 2D structure helps it to adhere tightly to surface imperfections, encourag-

ing improved lubrication and lowering the risk of surface damage. Furthermore, MXenes' excellent thermal conductivity allows for effective heat dissipation, which aids in temperature management and prevents excessive engine overheating [25,26]. The $Ti_3C_2T_x$ MXene nanoparticles also have intrinsic tribological qualities, such as strong load-bearing capacity and good anti-wear capabilities. Their inclusion in engine oil can result in lower frictional losses, increased fuel economy, and a longer engine life [27].

Until recently, various synthesis approaches have been developed to achieve MXene production. Conventional wet-chemical etching at room temperature, involving hazardous HF etchant, offers a simple and accessible method but a toxic handling environment, and lacks control over morphology and homogeneity [28,29]. Hydrothermal and solvothermal heating methods enable the formation of crystalline MXenes at controlled temperatures and offer versatility, but they require specialised equipment and longer reaction times [30–32]. On the other hand, the electrochemical process provides precise control over MXene properties, but is limited to precursor materials stable under electrochemical conditions [33]. While the minimal intensive layer delamination (MILD) synthesis approach offers safer handling conditions and well-delaminated MXene sheets with preserved morphology, the formation of MXene sheets can be relatively slow, leading to extended synthesis durations [28,34]. Notably, the microwave-assisted hydrothermal method presents a compelling advantage in the characterisation of MXenes [34,35]. By utilising microwave irradiation during the hydrothermal synthesis, this method offers rapid synthesis times, improved crystallinity, enhanced homogeneity, and controlled morphology of the resulting MXenes [34,36–38]. According to Numan et al. [34], using microwaves together with the hydrothermal method facilitates the efficient energy transfer and heating of the reaction mixture, promoting the formation of high-quality MXene layers. Unlike the conventional hydrothermal method, the microwave-assisted hydrothermal technique combines heat from microwave irradiation and the hydrothermal process, providing a short heating time and reducing heat losses [39,40]. Furthermore, the rapid synthesis and low operating temperature of the microwave-assisted hydrothermal method, which is from 35 to 200 °C [35], hinders the exposure of MXene to long and high heating temperature, which possibly increases the tendency of oxidation, as in the hydrothermal approach.

This work adopted a novel method to synthesise $Ti_3C_2T_x$ MXene nanoparticles with a variable interlayer spacing, utilising an advanced microwave-hidrothermal synthesis platform which significantly decreased synthesis time and energy consumption. This study aims to examine and understand the underlying process by which the addition of $Ti_3C_2T_x$ MXene improves base oil performance. Various characteristics, such as the coefficient of friction (COF), average wear scar diameter (WSD), oxidation induction time (OIT), and thermal conductivity, were carefully investigated to attain this aim. The ultimate goal is to understand better the impacts of $Ti_3C_2T_x$ MXene additions on engine oil behaviour, which might lead to new high-performance lubricants. Using $Ti_3C_2T_x$ MXene additives, the findings of this study will provide essential insights into the performance enhancement of engine oil, which demonstrate great promise in mitigating tribological problems and overcoming pollution challenges. Through concerted efforts and interdisciplinary research, we can pave the way for a cleaner and more sustainable future for our marine ecosystems.

2. Materials and Methods

2.1. Materials

Materials used to prepare the MXene powder included titanium aluminium carbide (Ti_3AlC_2, Mesh 400, 99.9%) purchased from Xiamen Tob New Energy Technology Co., Ltd., Xiamen City, Fujian Province, China, hydrochloric acid, HCl (37% v/v, Merck, Rahway, NJ, USA), lithium fluoride, LiF (300 mesh), and ethanol (96%) purchased from Sigma Aldrich, Petaling Jaya, Selangor, Malaysia. The lubricant oil used was outboard engine oil with certified TC-W specifications by National Marine Manufacturers Association, NMMA. All chemicals were of analytical grade and were used without further purification.

2.2. Synthesis of $Ti_3C_2T_x$ MXene

$Ti_3C_2T_x$ MXene was synthesised using an advanced microwave hydrothermal synthesis platform (Milestone, flexiWAVE, Sorisole (BG), Italy). $Ti_3C_2T_x$ MXene was produced in situ HF by combining LiF and HCl. A total of 2.5 M LiF was added and dissolved in 10 mL of 6 M and 9 M concentrated HCl in a Teflon tube to prepare a 6 M-$Ti_3C_2T_x$ MXene and 9 M-$Ti_3C_2T_x$ MXene, respectively. A total of 0.5 g of MAX phase was progressively added to the LiF/HCl solution, to avoid risky exothermic reactions. The mixture was then magnetically stirred for 30 min, followed by 30 min of sonication. The combined solution was then transferred into an advanced microwave hydrothermal for time-effective etching. Using an advanced microwave-assisted hydrothermal approach, synthesis was carried out at 30 °C with a reaction time of 10 min. Figure 1 shows the illustration of $Ti_3C_2T_x$ MXene synthesis via advanced microwave–hydrothermal synthesis. When the reaction was completed, the acidic mixture was washed and rinsed a few times with deionised water and ethanol, before being centrifuged for 5 min at 5000 rpm using a Sartorius centrifuge (Goettingen, Germany). The supernatant was discarded, and the washing process was repeated until a stable black MXene colloidal solution was attained. The MXene solution, which is devoid of the aluminium layer and any subsequent products, was then taken as pure MXene. After that, this solution was applied to the MXene layer's delamination or opening process. In order to obtain the MXene powder, a freeze dryer was used to carry out the freeze-drying process. The synthesis methodology has been adopted from our previous work [34,41].

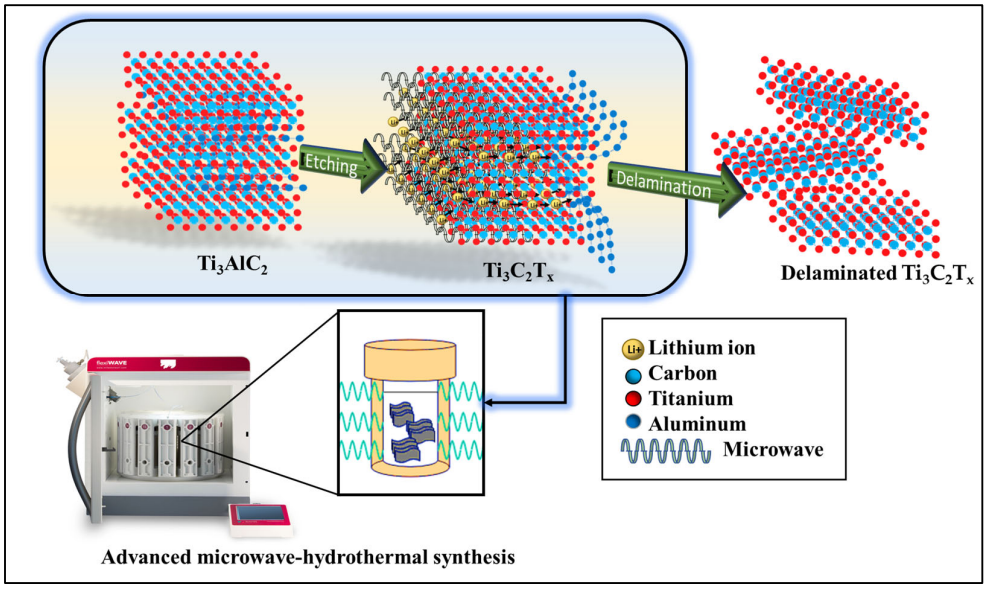

Figure 1. Schematic illustration of $Ti_3C_2T_x$ MXene synthesis via advanced microwave–hydrothermal synthesis.

2.3. Characterisation

The phase structure and crystallinity of as-synthesised 6 M-$Ti_3C_2T_x$ MXene and 9 M-$Ti_3C_2T_x$ MXene nanosheets were analysed using an X-ray diffractometer (XRD, BRUKER D8 advance) with Cu Kα radiation (U = 40 kV, I = 30 mA, and λ = 0.154 nm). The 2θ-degree patterns were observed between 5 and 80° at a 5°/min scanning rate. Energy-dispersive X-ray spectroscopy (EDX, Quanta 400F, Cambridge, MA, USA) was used to determine the elemental composition of the MXene. The morphology characterisation of $Ti_3C_2T_x$ MXene nanosheets was examined utilising field emission scanning microscopy (FESEM, ZEISS SUPRA 55VP).

2.4. Formulation of $Ti_3C_2T_x$ MXene Nanolubricant

The nanolubricant samples were formulated by dispersing 0.005 wt.%, 0.01 wt.%, and 0.05 wt.% as-synthesised 6 M-$Ti_3C_2T_x$ MXene and 9 M-$Ti_3C_2T_x$ MXene powder in 100 mL TC-W certified outboard engine oil by NMMA. In order to ensure homogenised dispersion of nanoparticles and obtain stability, oil samples were subjected to sonication using a water bath sonicator for 30 min and further homogenised for 10 min utilising a high shear lab mixer. For each concentration, three samples were prepared and repeatedly measured to minimise the errors and inconsistencies, ensure reliability and maintain quality control.

2.5. Physiochemical Characterisation of $Ti_3C_2T_x$ MXene Nanolubricant

A stability test was conducted using Zeta Potential (Malvern Zetasizer 3000HSA) for each oil sample, to ensure the stability of $Ti_3C_2T_x$ MXene nanolubricant and no MXene flocculation build-up in the oil. A viscometer (Viscometer SWM 3000, Anton Paar, Graz, Austria) was utilised to measure the density, kinematic viscosity, and viscosity index of the formulated 6 M-$Ti_3C_2T_x$ MXene and 9 M-$Ti_3C_2T_x$ MXene nanolubricant. The kinematic viscosity of the oil samples was measured at temperatures of 40 °C and 100 °C. Kinematic viscosity in the present study was calculated according to Equation (1):

$$v = \frac{\mu}{\rho} \tag{1}$$

where ν, μ and ρ represent kinematic viscosity, dynamic viscosity and density, respectively. The viscosity index (*VI*) is the rate of viscosity change as a function of temperature. In essence, *VI* is necessary to determine whether the lubricant satisfies the asset's requirements, depending on the operating temperature range. The *VI* was determined according to the standard ASTM D2270 and calculated using Equation (2):

$$VI = \frac{L - U}{L - H} \times 100 \tag{2}$$

where *U* denotes the oil's kinematic viscosity at 40 °C, whereas *L* and *H* are the reference oil's kinematic viscosities at 40 °C and 100 °C, respectively, as determined by ASTM D2270.

2.6. Four-Ball Tribotesting of $Ti_3C_2T_x$ MXene Nanolubricant

The tribological testing was conducted using a four-ball tribometer (DUCOM), following standard testing ASTM D 4172, to investigate the friction and wear properties of nanolubricant with different $Ti_3C_2T_x$ MXene concentrations. The temperature used was 75 °C, the rotational speed was 1200 rpm, and the applied load given to the other three balls was 392.5 N. The test was performed for 3600 s. Carbon–chromium steel balls were used in this test. Table 1 shows the mechanical properties of the balls used. After the testing, the image of the wear scar on the metal balls was analysed using field emission scanning electron microscopy and energy-dispersive X-ray spectroscopy (FESEM and EDX, Quanta 400F, Cambridge, MA, USA). The mechanical properties of the carbon-chromium steel balls used in the test are shown in Table 1.

The coefficient of friction was calculated using Equation (3):

$$\mu = 2.22707\frac{\tau}{\rho} \tag{3}$$

where μ represents the coefficient of friction, τ denotes the average frictional torque in kg-cm, and ρ is the load applied while performing the tribotest.

Table 1. Mechanical properties of the carbon-chromium steel ball-bearing used in four-ball tribotesting.

Mechanical Properties	Value
Hardness (H)	1 HRC
Density (ρ)	7.79 gm/cm^3
Surface roughness (Ra)	0.22

2.7. Oxidation Analysis of $Ti_3C_2T_x$ MXene Nanolubricant

MXene nanolubricants and outboard engine oil samples were measured to determine their oxidation induction time (OIT). The differential scanning calorimetry (DSC) method, following standard procedure ASTM 6186, was utilised to study the oxidative stability of nano marine oil. The tests were conducted using high-pressure differential scanning calorimeters (HP-DSC 250, from TA Instrument, Cheshire, UK). In this experiment, oxygen pressure was set and maintained at 200 psi throughout the experiment. A total of 3 mg of each sample was inserted into a standard aluminium pan as a test cell, while an empty pan was used as a reference. Both were used for oxidation testing and placed in a DSC cell. The DSC lid was closed, and oxygen was purged into the system until the pressure reached 200 psi. In the isothermal procedure, the measurements were performed at a temperature of 185 °C for 70 min. The DSC curve appeared in the form of exothermic heat flow during the initial state of the oxidation reaction, indicating the oxidation process. The oxidation induction time, which is the time required to begin the oxidation process of a sample, was determined from the DSC curve. Based on this curve, the point of intersection of the extrapolated baseline and the tangent line, which is the leading edge of the exothermal peak, represented the OIT.

2.8. Thermal Conductivity Analysis of $Ti_3C_2T_x$ MXene Nanolubricant

The good thermal conductivity of lubricating oil is the key to the excellent performance of the lubricating oil. The thermal conductivity of lubricating oil samples with different concentrations of $Ti_3C_2T_x$ MXene was evaluated using laser flash analysis, LFA HyperFlash, NETZSCH, Germany. In this experiment, samples were filled into the sample ring evenly. Before the sample holder components were assembled, the top and bottom sealing discs were sprayed with graphite to promote absorption. The sample was then subjected to laser flash analysis, LFA. Heating was applied from room temperature to 100 °C at a rate of 10 °C/min. The experiment was conducted in a nitrogen atmosphere.

3. Results and Discussions

3.1. Chemical and Structural Characterization of Nanomaterials

The phase structure, crystallinity, morphology and elemental composition of bulk MAX phase precursor and as-synthesised 9 M-$Ti_3C_2T_x$ MXene, as well as 6 M-$Ti_3C_2T_x$ MXene nanosheets, were characterised by XRD, FESEM, and EDX; these are presented in Figure 2. The XRD patterns in Figure 2A were observed to validate the formation of 9 M-$Ti_3C_2T_x$ MXene and 6 M-$Ti_3C_2T_x$ MXene from MAX phase Ti_3AlC_2. The XRD result evidently exhibits that the $Ti_3C_2T_x$ MXene is effectively attained from the etching and exfoliating of the MAX phase through advanced microwave-assisted hydrothermal synthesis. The XRD data for the MAX phase diffraction (002), (004), (101), (103), (104), (105), (109), and (110) planes are observed at 9.7°, 19.2°, 34.1°, 39.0°, 41.9°, 56.5°, and 60.4°, respectively, consistent with the standard (JCPDS No.52-0875). After going through the advanced microwave–hydrothermal synthesis, most of the sharp peaks at Ti_3AlC_2 almost disappeared, and $_a$ sharp diffraction peak at 9.64° 2θ, corresponding to the (002) diffraction plane, are gradually shifted from 9.64° to 6.13° and 6.54° for 9 M-$Ti_3C_2T_x$ MXene and 6 M-$Ti_3C_2T_x$ MXene, respectively. The (002) plane broadened and shifted towards a lower angle, suggesting that the grain size reduced and the nanosheet spacing of MXene increased, in agreement with the previous literature [34,42]. According to the Bragg formula, the c-lattice parameters for 9 M-$Ti_3C_2T_x$ MXene and 6 M-$Ti_3C_2T_x$ MXene are about 24.73 Å and 22.10 Å,

respectively. The result indicates that, with higher HCl concentration, in this case 9 M, more H^+ ions are provided by HCl to react with fluoride salt to form HF. Sufficient HF eases the etching of Al and expands the interlayer spacing between MXene sheets easily [43]. Furthermore, a higher amount of H^+ in 9 M HCl promotes hydrophilicity. H^+ attracts more water molecules to intercalate between MXene nanolayers during etching, resulting in an increased expansion of interlayer spacing compared to the lower concentration of HCl. Figure 2B,C,F depict the morphological structure of MAX phase Ti_3AlC_2, 9 M-$Ti_3C_2T_x$ MXene and 6 M-$Ti_3C_2T_x$ MXene, respectively, after going through etching and exfoliation with HCl/LiF via advanced microwave-assisted hydrothermal synthesis. In Figure 2B, the bulk MAX phase precursor Ti_3AlC_2 microstructure shows a solid and stacked multilayer nanosheet structure. In contrast, in Figure 2C,F, crumpled MXene sheets can be seen, signifying the exclusion of the Al element from packed MAX layers throughout the etching and exfoliation. The result demonstrates an effective formation of thin layers of 2D MXene nanosheets using an advanced microwave-assisted hydrothermal approach. The elemental mapping of both MXenes in Figure 2D,G shows the uniform spatial distribution of Ti, C, F, Cl, O, and Al. To validate the XRD and FESEM result, the EDX elemental spectrum in Figure 2E,H demonstrates that both MXene samples contain Ti, C, F and a small amount of O, Cl, and Al elements. The EDX analysis verifies the formation of MXene and the removal of most Al elements from the MAX phase.

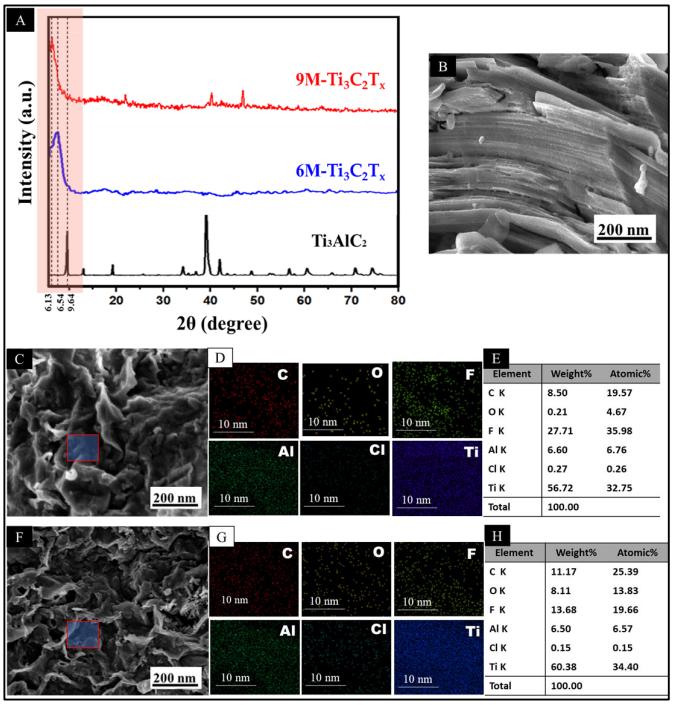

Figure 2. Structural characterisation of as-synthesised $Ti_3C_2T_x$ MXene. (**A**) XRD diffractogram of MAX phase, 9 M-$Ti_3C_2T_x$ MXene and 6 M-$Ti_3C_2T_x$ MXene. (**B**) FESEM micrographs of MAX phase. (**C**) FESEM micrographs of 9 M-$Ti_3C_2T_x$ MXene. (**D**) 9 M-$Ti_3C_2T_x$ MXene corresponding EDX elemental mapping. (**E**) Elemental composition of 9 M-$Ti_3C_2T_x$ MXene calculated from EDX analysis. (**F**) FESEM micrographs of 6 M-$Ti_3C_2T_x$ MXene. (**G**) Corresponding EDX elemental mapping of 6 M-$Ti_3C_2T_x$ MXene. (**H**) EDX spectra of 9 M-$Ti_3C_2T_x$ MXene and 6 M-$Ti_3C_2T_x$ MXene, respectively.

3.2. Physiochemical Characterisation of Nanolubricant

The zeta potential measures the strength of the electrokinetic potential, such as the attractive and repulsive interactions between particles suspended in a dispersion [44,45]. The size of the zeta potential value will determine whether the dispersion is relatively stable. The larger the absolute magnitude of the zeta potential, the stronger the dispersion will resist aggregation, resulting in a more extended period of stability. On the other hand,

the dispersion is more likely to coagulate, and its stability time is shortened when the absolute value of the zeta potential is closer to 0 mV. Figure 3A explains the stability ranges of the zeta potential. For zeta potential values between 0 and ±5 mV, the dispersed phase strongly tends to agglomerate; for values between ±10 and ±30 mV, an incipient instability is indicated; for values between ±30 and ±40 mV, moderate stability is identified; for values between ±40 and ±60 mV, good stability is specified; and for values higher than ±61 mV, excellent stability is signified. Thus, nanolubricant stability is significantly affected by their electrokinetic properties. Due to the strong repulsive forces exerted by the high surface charge density, the probability of flocculation is reduced [45–47].

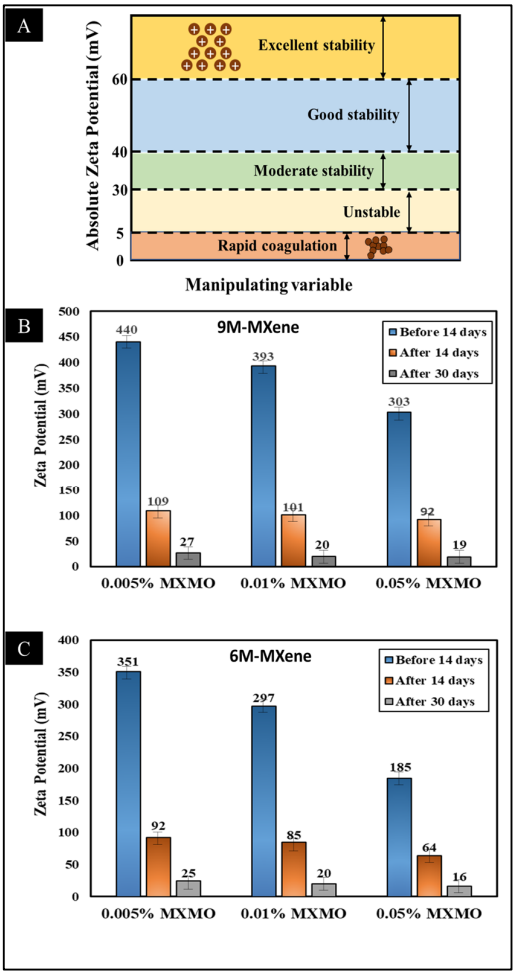

Figure 3. (**A**) Schematic illustration explaining stability and zeta potential ranges. (**B**,**C**) The zeta potential of 9 M-$Ti_3C_2T_x$ MXene and 6 M-$Ti_3C_2T_x$ MXene nanolubricants before 14 days, after 14 days, and after 30 days.

Figure 3B shows the zeta potential of 9 M-$Ti_3C_2T_x$ MXene and 6 M-$Ti_3C_2T_x$ MXene nanolubricant before 14 days, after 14 days, and after 30 days. In this study, the zeta potential of MXene nanolubricant dispersion shows >61 mV, presenting the excellent stability of both 9 M-$Ti_3C_2T_x$ MXene and 6 M-$Ti_3C_2T_x$ MXene, regardless of the concentration, before and after 14 days. However, the stability of MXene nanolubricant deteriorates after 30 days, where zeta potential is less than 30 mV, indicating coagulation of MXene nanoparticles occurred after one month. It is also observed that the zeta potential value almost linearly decreased with $Ti_3C_2T_x$ MXene concentration. This suggests that there is restricted nanoparticle mobility at higher concentrations, which inhibits the building of the energy barrier and causes particle agglomeration and sedimentation. In other words, the stearic repulsion between nanoparticles rises with concentration, causing them to aggregate and

reduce the zeta potential value. According to Said et al. [44], when particle concentration rises, the average static surface-to-surface spacing decreases, which causes the particle to cluster. Thus, high spacing between the particles for 9 M-$Ti_3C_2T_x$ MXene and 6 M-$Ti_3C_2T_x$ MXene would be ineffective.

Figure 4 presents the kinematic viscosity of MO, 9 M-$Ti_3C_2T_x$ MXene, and 6 M-$Ti_3C_2T_x$ MXene nanolubricants tested at 40 °C and 100 °C. The results show a trend of reduction in kinematic viscosity when the temperature rises. With the increment in temperature, the thermal energy induces higher kinetic energy towards molecules, which causes rapid and mobile movement. The attractive binding energy between the molecules decreases, significantly reducing the kinematic viscosity [11,48]. Therefore, the kinematic viscosity findings show that MXene nanoparticles assist in modifying the viscosity of the nanolubricant when the temperature changes. In addition, the kinematic viscosity shows little increase after adding different concentrations of MXene nanoparticles. There are no significant changes between the kinematic viscosity of 9 M-$Ti_3C_2T_x$ MXene and 6 M-$Ti_3C_2T_x$ MXene nanolubricants, due to minimal differences in interlayer spacing of MXene nanosheets, which is considered a negligible factor influencing the kinematic viscosity of the lubricant. Thus, the reduction in kinematic viscosity suggests that MXene nanoparticles work as an increasing catalyst as the concentration of MXene increases, regardless of the size of the c-lattice parameter.

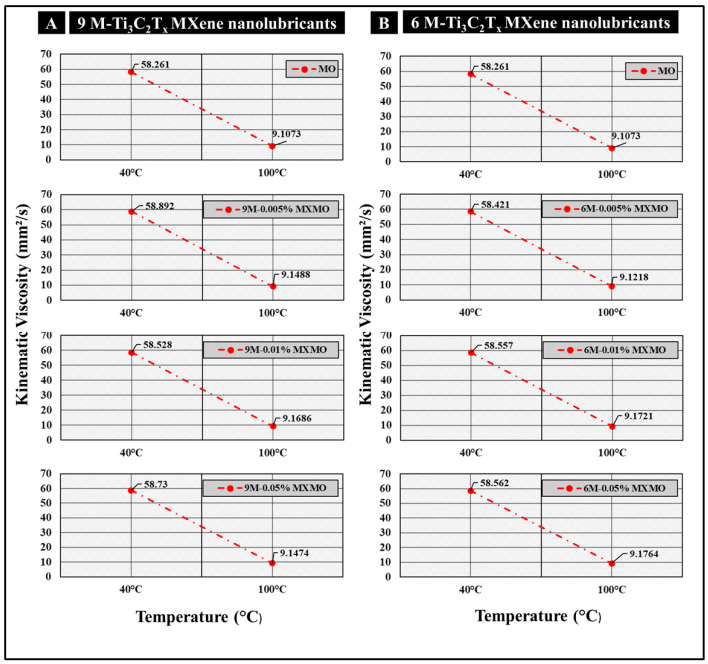

Figure 4. Kinematic viscosity at 40 °C and 100 °C of (**A**) 9 M-$Ti_3C_2T_x$ MXene nanolubricant and (**B**) 6 M-$Ti_3C_2T_x$ MXene nanolubricant.

Furthermore, the demand for engine oils with higher fuel-saving efficiency has been driven by the need to reduce CO_2 emissions from marine transportation. The implementation can be anticipated by developing an engine oil with a high viscosity index (VI). In general, engine oils become more viscous at lower temperatures, increasing engine drag. High VI reduced oil viscosity at lower temperatures, improving fuel-saving efficiency. Figure 5 exhibits the variation in viscosity index with different concentrations of 9 M-$Ti_3C_2T_x$ MXene and 6 M-$Ti_3C_2T_x$ MXene nanolubricants. Figure 5 reveals that adding 0.01 wt.% of 9 M-$Ti_3C_2T_x$ MXene and 6 M-$Ti_3C_2T_x$ MXene elevated the VI of base oil by 1.14% and 0.76%, respectively. Compared to base oil, MXene nanolubricants show slightly higher VI, which offers low viscosity change at varying temperatures, improved thinning resistance, and preserved protective oil film strength under high pressure and temperature. This finding demonstrates that using MXene nanoparticles in outboard engine oil poten-

tially enhances the viscosity index and increases engine oil preference for high-temperature use.

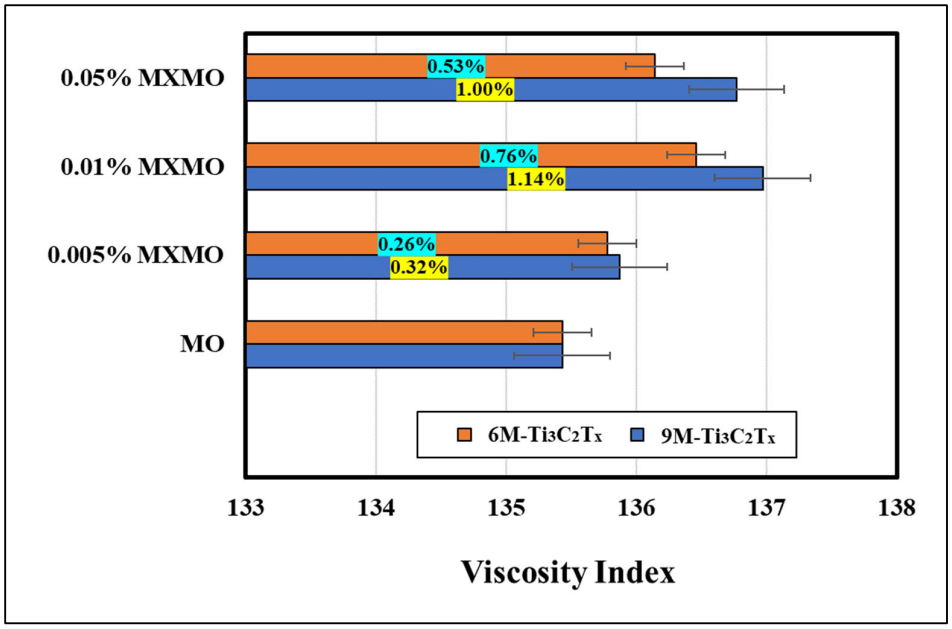

Figure 5. Viscosity index of the nanolubricant with 9 M-$Ti_3C_2T_x$ MXene and 6 M-$Ti_3C_2T_x$ MXene nanolubricant.

3.3. Tribological Analysis of $Ti_3C_2T_x$ MXene Nanolubricant

As is well known, adding excessive or insufficient nano-additives with the ideal interlayer spacing of MXene can cause lubricating oil performance to be compromised. The coefficient of friction (COF) and average wear scar diameter (WSD) of MXene nanolubricant with different interlayer spacing and concentrations of $Ti_3C_2T_x$ MXene nanoparticles in outboard engine oil are therefore used to determine the optimal interlayer spacing and concentration. The results are shown in Figure 6. As depicted in Figure 6A, the COF of the base oil is 0.1252. The COF first decreased when 9 M-0.005 wt.% and 9 M-0.01 wt.% of MXene were added to the base oil. Nanolubricant with 9 M-0.005 wt.% of $Ti_3C_2T_x$ MXene contains an adequate number of nanoparticles to promote formation of a protective layer between the mating surfaces. Building a tribofilm comprised of nanosheets helps mitigate the friction caused by the slippage of the individual layers of nanosheets [49]. Further addition of MXene concentration, 9 M-0.01 wt.%, shows a significant decrement of COF, possibly attributed to the optimal amount of nanosheets to form a homogenous tribofilm during sliding and deformation of individual nanosheets, which results in a reduction in friction between mating surfaces. However, the COF started to increase when the concentration reached up to 9 M-0.05 wt.%, which can be attributed to the flocculation of $Ti_3C_2T_x$ MXene nanoparticles, dramatically expanding the nanoparticle size. Consequently, the nanoparticles cannot enter the tiny space between the friction contact, leading to higher COF [8,49,50].

It should be noted that adding 6 M-$Ti_3C_2T_x$ MXene, with lower interlayer spacing, into base oil exhibits the same COF reduction trend, with an insignificant percentage of COF decrement (less than 10%). This may be due to deficient interlayer spacing to facilitate lower shear strength, which promotes better lubricity to reduce friction, compared to 9 M-$Ti_3C_2T_x$ MXene nanoparticles with higher interlayer spacing. On the other hand, 6 M-0.01 wt.% $Ti_3C_2T_x$ MXene nanolubricant also demonstrates the highest improvement in COF amongst other 6 M concentrations, suggesting that 0.01 wt.% of MXene is the optimal amount to establish a uniform tribolayer between mating surfaces. Overall, MXene additive nanolubricants with varying concentrations and interlayer spacing assist in reducing COF and wear, showing potential as an anti-friction and anti-wear agent. In evaluation with other

reported studies, a comparison table showing our results and the tribological performance of other nanomaterials is attached in Appendix A.

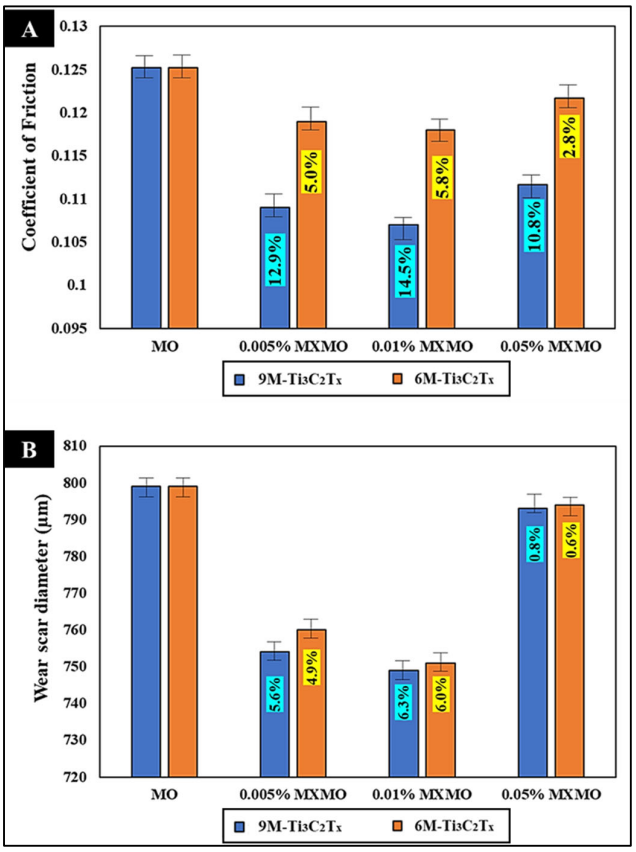

Figure 6. (**A**) The coefficient of friction of 9 M-$Ti_3C_2T_x$ MXene and 6 M-$Ti_3C_2T_x$ MXene nanolubricants. (**B**) The average wear scar diameter of 9 M-$Ti_3C_2T_x$ MXene and 6 M-$Ti_3C_2T_x$ MXene nanolubricants.

Figure 6B presents the average wear scar diameter (WSD) with varying MXene additive concentrations in outboard engine oil. The WSD of the ball without any addition of MXene additive is 818 µm. Figure 6B shows that 0.005 wt.%–0.05 wt.% of 9 M-and 6 M-$Ti_3C_2T_x$ MXene additive dispersed in outboard engine oil improved WSD from 0.6% to 6.3% in comparison with base oil, while higher improvement in WSD is shown by 9 M-$Ti_3C_2T_x$ MXene nanolubricant compared to 6 M-$Ti_3C_2T_x$ MXene nanolubricant; however, no significant difference in WSD reduction associated to the variation in interlayer spacing. The result also demonstrates 0.01 wt.% 9 M-$Ti_3C_2T_x$ MXene additive establishes the lowest average WSD. The decrease of WSD of 0.01 wt.% 9 M-$Ti_3C_2T_x$ MXene is attributed to the forming of a thin lubricating layer between the contact surfaces, which helps minimise contact pressure and frictional torque [47]. Furthermore, the occurrence of the mending effect can promote the reduction in the average WSD. This effect occurs when the 2D nanoparticles accumulate and deposit in the tiny cracks and ridges of mating surfaces, smoothing them out and lowering the average WSD. This mechanism and result are in agreement with former studies [8,41,51,52].

These findings were further confirmed with FESEM and EDX analyses on the steel ball surface, as shown in Figure 7. In Figure 7A, the surface of the ball bearing with base oil with no addition of MXene shows darker concentric grooves, indicating a deeper furrow. The lowest WSD was chosen to compare with the WSD of a non-additive nanolubricant. In Figure 7B, with 0.01 wt.% 9 M-$Ti_3C_2T_x$ MXene additive, the scar under FESEM observation appears to be brighter, representing a shallower furrow. Bright and smooth wear tracks appeared when the lubricant with $Ti_3C_2T_x$ MXene nanoparticles was mixed, demonstrating

a reduction in the contact surfaces between the steel balls. It is hypothesised that MXene nanosheets can easily slide and infiltrate the oil surface due to their two-dimensional structure. Additionally, nanosheets offer a continuous layer on sliding surfaces because of their excellent contact adherence. This behaviour is associated with the mending property of $Ti_3C_2T_x$ MXene. The nanoparticles repair the scratched and worn surfaces by being deposited into worn surfaces, while building a protective layer to eliminate direct contact between the two contact surfaces, minimising the wear scar diameter. The adherence of $Ti_3C_2T_x$ MXene nanoparticles on the cracks assists in a reduction in the depth of the grooves, as evidenced in Figure 7D by the presence of Ti element in the EDX elemental spectrum of the scar on the steel ball. In comparison, no Ti element was observed on the steel ball scar with the base oil lubricant in Figure 7C. The experimental tribological results above suggest that, with an optimal concentration of 0.01 wt% $Ti_3C_2T_x$ MXene in the outboard engine oil, COF and WSD can be significantly improved.

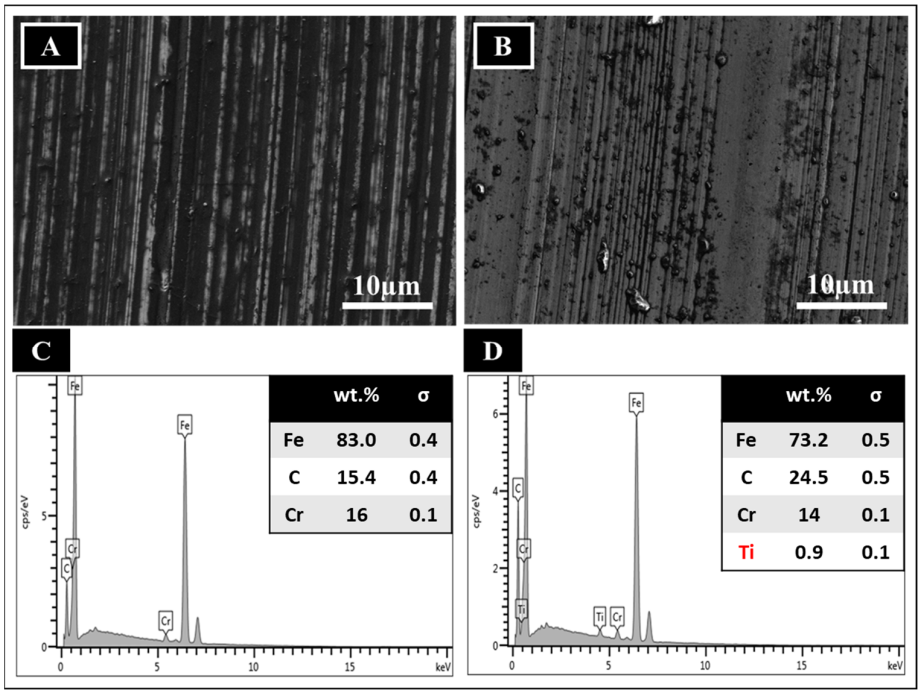

Figure 7. FESEM images of wear scar diameter with (**A**) base oil and (**B**) 9 M-0.01 wt.% MXMO. EDX elemental spectra of the wear scar with (**C**) base oil and (**D**) 9 M-0.01 wt.% MXMO.

According to the previous study, the development of tribofilm and the mending effect is the fundamental mechanism for reducing frictional wear in the case of $Ti_3C_2T_x$ MXene nanolubricant. The two-dimensional plane structure of $Ti_3C_2T_x$ MXene allows it to glide between the oil surface easily. Furthermore, when the concentration of $Ti_3C_2T_x$ MXene grows, it will agglomerate and precipitate, increasing wear and friction between mating surfaces. The wear process of $Ti_3C_2T_x$ MXene nanosheets is related to the segregation of interlayers into different layers [53,54] due to reduced van der Waals or Coulombic repulsive interactions at contact points. Thus, a higher interlayer spacing with lower van der Waals interaction easily disintegrated into individual layers and quickly adhered to the worn surface, promoting better lubricity to the contact surface, resulting in higher improvement in COF and wear compared to $Ti_3C_2T_x$ MXene with lower interlayer spacing, as supported by the previous literature [55]. Thus, the findings show that adding $Ti_3C_2T_x$ MXene to the lubricant substantially enhances its tribological properties.

3.4. Oxidation Analysis of $Ti_3C_2T_x$ MXene Nanolubricant

High loads and temperatures and continuous air contact are the main contributors to the oxidation of lubricants in the transportation industries, including marine transportation. Oxidation accelerates the degradation of base oils and additives, decreasing their efficiency, performance, and life expectancy. Figure 8 displays the oxidation induction time (OIT) of 9 M-$Ti_3C_2T_x$ MXene nanolubricant since 9 M-$Ti_3C_2T_x$ MXene nanolubricant consistently shows better physiochemical and tribological properties compared to 6 M-$Ti_3C_2T_x$ MXene nanolubricant. The results show OIT enhancement by adding 9 M-$Ti_3C_2T_x$ MXene to the outboard engine oil. Compared with base oil, the OIT improves by 35.1%, 54.8% and 30.1% for 0.005 wt.%, 0.01 wt.% and 0.05 wt.%, respectively. Amongst other concentrations of nanolubricant formulation, the nanolubricant with 0.01 wt.% 9 M-$Ti_3C_2T_x$ MXene nanoparticles was found to enhance theOIT by the most suggesting that this concentration is the optimal concentration of MXene additive in the outboard engine oil, which offers the anti-oxidation effect that can expand lubricant service lifespan.

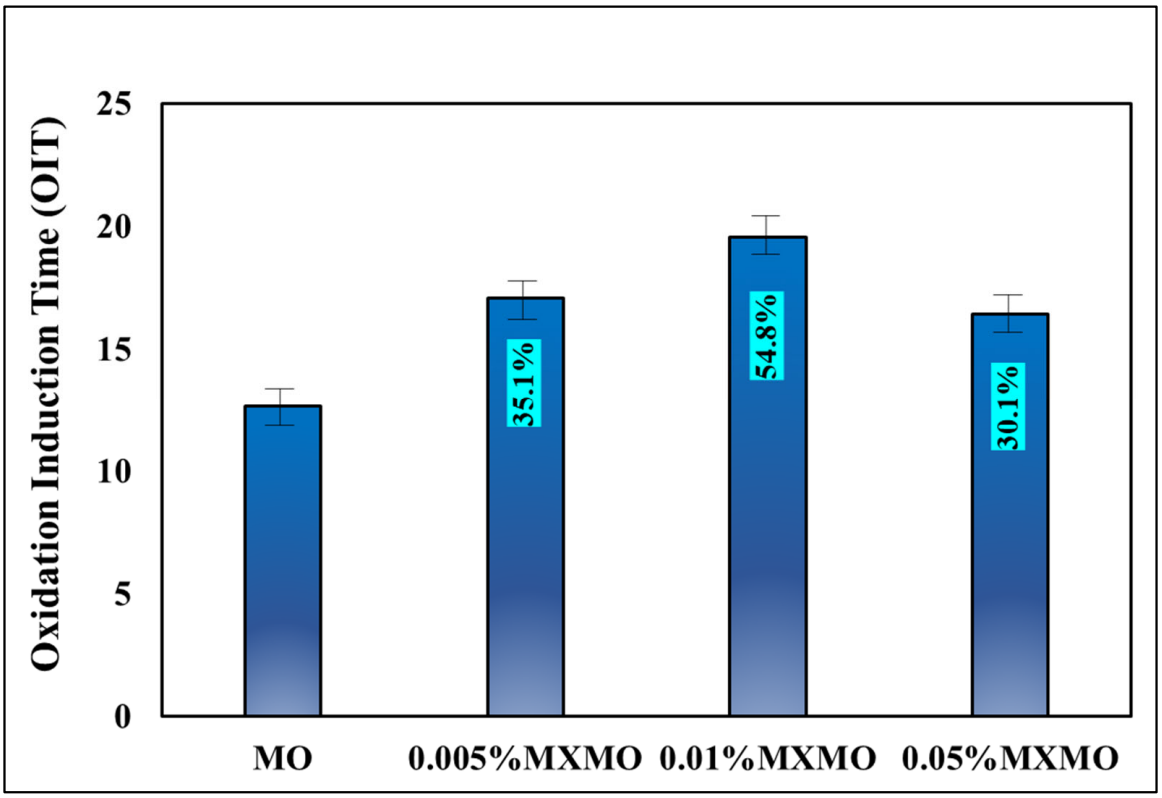

Figure 8. The oxidation induction time (OIT) of nanolubricants with different MXene concentrations.

3.5. Thermal Conductivity Analysis of $Ti_3C_2T_x$ MXene Nanolubricant

In order to reduce the heat generated by the moving components of an engine and overcome mechanical fatigue, a good lubricant is required to possess a high level of thermal conductivity [12]. The thermal conductivities of $Ti_3C_2T_x$ MXene with TC-W certified outboard engine oil samples for different concentrations are plotted in Figure 9A as a function of temperature from 40 °C to 100 °C. The influence of concentration and temperature on the thermal conductivity of $Ti_3C_2T_x$ MXene nanolubricant was analysed. The standard deviations for the thermal conductivity of the samples are ±0.002. The result shows that the thermal conductivity of $Ti_3C_2T_x$ MXene nanolubricant samples almost linearly increased with $Ti_3C_2T_x$ MXene concentration from 0.005 wt.% to 0.05 wt.% in engine oil. The high concentration of $Ti_3C_2T_x$ MXene dramatically increases with the content of $Ti_3C_2T_x$ MXene nanoparticles in the oil sample. The sample of oil with 0.05 wt.% of $Ti_3C_2T_x$ MXene exhibits the maximum thermal conductivity, which is 0.14 W/m K at 40 °C, and increases

to 0.28 W/m K at 100 °C, with 59% and 69.7% of thermal conductivity enhancement, respectively, as shown in Figure 9B. With higher concentrations of MXene and uniformly dispersed ultra-high thermal conductivity nanoparticles, the nanoparticles are easily connected with each other to enhance heat dissipation. In other words, the molecular collisions between the base oil and more nanoparticles led to higher thermal conductivity. [49,56,57]. In addition, $Ti_3C_2T_x$ MXene nanosheets offer a high aspect ratio due to the size and layer morphology, which provide an increased contact interface to improve the thermal conductivity of lubricants with a higher amount of MXene nanoparticles [12,48]. Furthermore, the improvement in thermal conductivity of $Ti_3C_2T_x$ MXene nanolubricant is associated with the vast basal plane of $Ti_3C_2T_x$ MXene sheets present in outboard engine and the intense heat conductivity across the basal plane of $Ti_3C_2T_x$ MXene nanoflakes [58,59]. These planes have a high density of delocalised electrons, and can transfer heat quickly and efficiently through the material, which significantly improves the thermal conductivity of $Ti_3C_2T_x$ MXene nanolubricant.

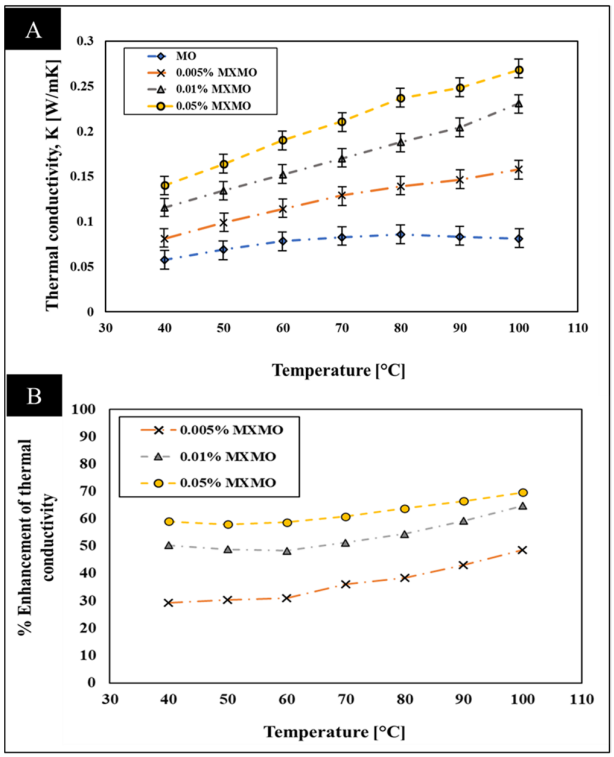

Figure 9. (**A**) Thermal conductivity of $Ti_3C_2T_x$ MXene with outboard engine oil as a function of temperature for the varying MXene concentrations of 0.005, 0.01, and 0.05 wt.%. (**B**) Percentage of thermal conductivity enhancements of $Ti_3C_2T_x$ MXene with outboard engine oil as a function of temperature for different concentrations.

Figure 9 shows that thermal conductivity also increases with temperature elevation. The molecules in base oil obtain a high-velocity vibration as the temperature rises. Dispersing $Ti_3C_2T_x$ MXene nanoparticles in outboard engine oil also induces a random collision; striking and hitting nanoparticle surfaces causes the Brownian motion effect. Under the high-temperature condition, the $Ti_3C_2T_x$ MXene nanoparticles gain more energy, and the Brownian motion effect becomes more intense, which results in a fascinating phenomenon known as thermophoresis [49,59,60]. Thermophoresis is the movement of particles brought on by a temperature gradient in the fluid. Brownian motion and thermophoresis both promote particle collision, though thermophoresis may sometimes have a more substantial impact. These particle collisions often result in an increase in thermal conductivity.

It is also worth noting that, at low temperatures, the lubricant's viscosity is higher, which can limit the mobility of the $Ti_3C_2T_x$ MXene nanosheets in the lubricant. This can

decrease the effect of Brownian motion and the lubricant's thermal conductivity because the $Ti_3C_2T_x$ MXene nanoparticle transport between the MXene layers is decelerated. As the temperature increases, the lubricant's viscosity decreases, allowing for greater mobility of the $Ti_3C_2T_x$ MXene nanosheets. This leads to an increase in the thermal conductivity of the lubricant attributed to the high Brownian motion effect [61–63].

4. Conclusions

The current work has effectively established $Ti_3C_2T_x$ MXene nanoparticles as a potent anti-friction, anti-oxidant, and excellent thermal conductor additive with improved tribological, oxidation, and thermal conductivity performance in outboard engine oil. In the tribological analysis, nanolubricant with 0.01 wt.% concentration of $Ti_3C_2T_x$ MXene nanoparticles shows outstanding results in reducing the friction coefficient and average wear scar diameter, with 14.5% and 6.3% decrement, respectively, compared to the base oil. This is due to the tribofilm and mending effect, which promotes the formation of a protective film between the frictional surfaces and the deposition of nanoparticles in the cracks and ridges, decreasing the COF and average WSD. Furthermore, the addition of 0.01 wt.% $Ti_3C_2T_x$ MXene nanoparticles depict significant increases in OIT by 54.8% compared to base oil, revealing its anti-oxidation effect that can extend lubricant service duration. For the thermal conductivity analysis, the deployment of $Ti_3C_2T_x$ MXene nanoparticles shows an increasing trend in thermal conductivity as the number of nanoparticles increases. This can be explained by the high aspect ratio and the large basal plane of $Ti_3C_2T_x$ MXene nanoparticles, the effect of Brownian motion, and the thermophoresis phenomenon, which enhanced the thermal conductivity with increasing nanoparticles and temperature.

Author Contributions: Conceptualisation, H.A.Z., M.J.G., M.K. and A.K.R.; methodology, H.A.Z., M.K., T.N. and A.K.R.; formal analysis, H.A.Z., W.W.P. and R.W.; writing—original draft preparation, H.A.Z.; writing—review and editing, T.N., F.E. and O.G.; visualisation, H.A.Z., F.E. and O.G.; supervision, M.J.G., M.K. and A.K.R.; project administration, M.J.G. and M.K.; funding acquisition, M.J.G. and M.K. All authors have read and agreed to the published version of the manuscript.

Funding: This research was funded by the Ministry of Higher Education Malaysia and Universiti Kebangsaan Malaysia (grant number FRGS/1/2018/TK03/UKM/02/8) and also the international network research grant scheme from Sunway University, Malaysia (STR-IRNGS-SET-GAMRG-01-2022).

Data Availability Statement: Not applicable.

Conflicts of Interest: The authors declare no conflict of interest.

Appendix A

Material	Base Fluid	Concentration	Enhancement of Tribological Properties		Reference
			COF	Wear	
MXene $Ti_3C_2T_X$ nanosheets	DI- H_2O (AP30-$Ti_3C_2T_X$)	0.8 mg/mL	34.74%	45.58%	[64]
MXene $Ti_3C_2T_X$	DI- H_2O	5 wt.%	20%	48%	[65]
MXene $Ti_3C_2T_X$	PAO8 base oil	0.8 wt.%	9.5%	7.7%	[66]
$Ti_3C_2T_X$	Outboard oil	0.01 wt.%	0.8%	-	[1]
$TiO_2/Ti_3C_2T_X$	Oil	1.0 wt.%	29.1% (with 20N load)	Depth: 30 µm Width: 280 µm	[67]
$Ti_3C_2(OH)_2$	100SN base oil	1.0 wt.%	around 20% (with 15N load)	-	[68]
$Ti_3C_2T_X$	Liquid paraffin	1.0 wt.%	49.6%	-	[69]
KTO-$Ti_3C_2T_x$	PAO8 base oil	1.0 wt.%	30.6%	-	[55]

TDPA-Ti_3C_2	Castor oil	0.1 wt.%	27.9%	55.1%	[70]
DDP-Ti_3C_2Tx	500SN base oil	0.3 wt.%	COF: 0.11	87%	[71]
MXenes/MoS_2 heterojunction	Liquid paraffin	5.0 wt.%	39%	-	[72]
$Ti_3C_2T_x/MoS_2$ heterojunction	150SN base oil	0.3 wt.%	39%	85%	[73]
MXene-HS	PAO 10	1.0 wt.%	COF: 0.12	82%	[74]
Hybrid MoS_2@Ti_3C_2	SAE 5W-40-based engine oil	0.05 wt.%	13.9%	23.8%	[47]
MoS_2	SAE 20W50 diesel engine oil	0.01 wt.%	19.24%	19.52%	[49]
WS_2	Base oil + PVP surfactant	1.0 wt.%	33%	45%	[75]
Multi-layered graphene	PAO2 oil	0.05 wt.%	78%	16%	[76]
Graphene nanoplatelets (GNPs)	Palm oil TMP	0.05 wt.%	5%	15%	[77]
Graphene nanoparticle (GP)	Synthetic oil, PAO4	0.01 wt.%	78% (at 60–100 °C)	90% (at 60–100 °C)	[78]
Graphene	PAO4 oil	0.01 wt.%	50%	greater than 50%	[79]
Graphene	Vegetable oil	-	From 0.0825 to 0.0714	From 414 to 374	[80]
GO	DI-H2O		26.1%	39.4%	[81]
GO	DI-H2O	0.1 wt.%	0.03 (2.3 times lower than 0.5 wt% ND)	-	[82]
GO	DI-H2O	0.1 wt.%	COF: 0.05	No obvious wear after 60 000 cycles	[83]
CNT	Pure palm oil	2 wt.%	COF: 0.121 (APE-10)	-	[84]
MXene $Ti_3C_2T_X$	TC-W outboard engine oil	0.01 wt.%	14.5%	6.3%	Our work

References

1. Rasheed, A.K.; Khalid, M.; Nor, A.F.; Wong, W.Y.; Duolikun, T.; Natu, V.; Barsoum, M.W.; Leo, B.F.; Zaharin, H.A.; Ghazali, M.J. MXene-Graphene Hybrid Nanoflakes as Friction Modifiers for Outboard Engine Oil. In Proceedings of the IOP Conference Series: Materials Science and Engineering, Chennai, India, 25–26 September 2020; Volume 834, p. 012039. [CrossRef]
2. Anh Tran, T. Some Methods to Prevent the Wear of Piston-Cylinder When Using Low Sulphur Fuel Oil (LSFO) for All Ships Sailing on Emission Control Areas (ECAs). In *Diesel and Gasoline Engines*; IntechOpen: London, UK, 2020.
3. UNEP (United Nations Environment Programme) Marine Pollution. Available online: https://www.unep.org/explore-topics/oceans-seas/ (accessed on 16 May 2023).
4. Chen, C.; Saikawa, E.; Comer, B.; Mao, X.; Rutherford, D. Ship Emission Impacts on Air Quality and Human Health in the Pearl River Delta (PRD) Region, China, in 2015, with Projections to 2030. *GeoHealth* **2019**, *3*, 284–306. [CrossRef]
5. UN (United Nation) Transforming Our World: The 2030 Agenda for Sustainable Development. Available online: https://sdgs.un.org/2030agenda (accessed on 16 May 2023).
6. Ali, Z.A.A.A.; Takhakh, A.M.; Al-Waily, M. A Review of Use of Nanoparticle Additives in Lubricants to Improve Its Tribological Properties. *Mater. Today Proc.* **2022**, *52*, 1442–1450. [CrossRef]
7. Ng, B.Y.S.; Ong, H.C.; Lau, H.L.N.; Ishak, N.S.; Elfasakhany, A.; Lee, H.V. Production of Sustainable Two-Stroke Engine Biolubricant Ester Base Oil from Palm Fatty Acid Distillate. *Ind. Crops Prod.* **2022**, *175*, 114224. [CrossRef]
8. Zaharin, H.A.; Ghazali, M.J.; Thachnatharen, N.; Ezzah, F.; Walvekar, R.; Khalid, M. Progress in 2D Materials Based Nanolubricants: A Review. *FlatChem* **2023**, *38*, 100485. [CrossRef]
9. Ji, Z.; Zhang, L.; Xie, G.; Xu, W.; Guo, D.; Luo, J.; Prakash, B. Mechanical and Tribological Properties of Nanocomposites Incorporated with Two-Dimensional Materials. *Friction* **2020**, *8*, 813–846. [CrossRef]
10. Rosenkranz, A.; Liu, Y.; Yang, L.; Chen, L. *2D Nano-Materials beyond Graphene: From Synthesis to Tribological Studies*; Springer International Publishing: Berlin/Heidelberg, Germany, 2020; Volume 10, ISBN 0123456789.
11. Al-Janabi, A.S.; Hussin, M.; Abdullah, M.Z. Stability, Thermal Conductivity and Rheological Properties of Graphene and MWCNT in Nanolubricant Using Additive Surfactants. *Case Stud. Therm. Eng.* **2021**, *28*, 101607. [CrossRef]
12. Yang, L.; Mao, M.; Huang, J.N.; Ji, W. Enhancing the Thermal Conductivity of SAE 50 Engine Oil by Adding Zinc Oxide Nano-Powder: An Experimental Study. *Powder Technol.* **2019**, *356*, 335–341. [CrossRef]

13. Anantha Kumar, K.; Sandeep, N.; Samrat, S.P.; Ashwinkumar, G.P. Effect of Electromagnetic Induction on the Heat Transmission in Engine Oil-Based Hybrid Nano and Ferrofluids: A Nanotechnology Application. *Proc. Inst. Mech. Eng. Part E J. Process Mech. Eng.* **2022**. [CrossRef]
14. Manu, B.R.; Gupta, A.; Jayatissa, A.H. Tribological Properties of 2D Materials and Composites—A Review of Recent Advances. *Materials* **2021**, *14*, 1630. [CrossRef]
15. Thachnatharen, N.; Khalid, M.; Arulraj, A.; Sridewi, N. Tribological Performance of Hexagonal Boron Nitride (HBN) as Nano-Additives in Military Grade Diesel Engine Oil. *Mater. Today Proc.* **2022**, *50*, 70–73. [CrossRef]
16. Liu, Y.; Dong, Y.; Zhang, Y.; Liu, S.; Bai, Y. Effect of Different Preparation Processes on Tribological Properties of Graphene. *Nanomater. Nanotechnol.* **2020**, *10*, 1847980420946655. [CrossRef]
17. Yi, S.; Li, J.; Liu, Y.; Ge, X.; Zhang, J.; Luo, J. In-Situ Formation of Tribofilm with Ti3C2Tx MXene Nanoflakes Triggers Macroscale Superlubricity. *Tribol. Int.* **2021**, *154*, 106695. [CrossRef]
18. Ramanavicius, S.; Ramanavicius, A. Progress and Insights in the Application of MXenes as New 2D Nanomaterials Suitable for Biosensors and Biofuel Cell Design. *Int. J. Mol. Sci.* **2020**, *21*, 9224. [CrossRef] [PubMed]
19. Naguib, M.; Mochalin, V.N.; Barsoum, M.W.; Gogotsi, Y. 25th Anniversary Article: MXenes: A New Family of Two-Dimensional Materials. *Adv. Mater.* **2013**, *26*, 992–1005. [CrossRef]
20. Naguib, M.; Come, J.; Dyatkin, B.; Presser, V.; Taberna, P.-L.; Simon, P.; Barsoum, M.W.; Gogotsi, Y. MXene: A Promising Transition Metal Carbide Anode for Lithium-Ion Batteries. *Electrochem. Commun.* **2012**, *16*, 61–64. [CrossRef]
21. Anasori, B.; Lukatskaya, M.R.; Gogotsi, Y. 2D Metal Carbides and Nitrides (MXenes) for Energy Storage. *Nat. Rev. Mater.* **2017**, *2*, 16098. [CrossRef]
22. Rosenkranz, A.; Righi, M.C.; Sumant, A.V.; Anasori, B.; Mochalin, V.N. Perspectives of 2D MXene Tribology. *Adv. Mater.* **2023**, *35*, 2207757. [CrossRef] [PubMed]
23. Cai, M.; Yan, H.; Song, S.; He, D.; Lin, Q.; Li, W.; Fan, X.; Zhu, M. State-of-the-Art Progresses for Ti3C2Tx MXene Reinforced Polymer Composites in Corrosion and Tribology Aspects. *Adv. Colloid Interface Sci.* **2022**, *309*, 102790. [CrossRef]
24. Miao, X.; Li, Z.; Liu, S.; Wang, J.; Yang, S. MXenes in Tribology: Current Status and Perspectives. *Adv. Powder Mater.* **2023**, *2*, 100092. [CrossRef]
25. Wyatt, B.C.; Rosenkranz, A.; Anasori, B. 2D MXenes: Tunable Mechanical and Tribological Properties. *Adv. Mater.* **2021**, *33*, 2007973. [CrossRef]
26. Zhou, Y.; Liu, M.; Wang, Y.; Yuan, J.; Men, X. Significance of Constructed MXene@Ag Hybrids for Enhancing the Mechanical and Tribological Performance of Epoxy Composites. *Tribol. Int.* **2022**, *165*, 107328. [CrossRef]
27. Parra-Muñoz, N.; Soler, M.; Rosenkranz, A. Covalent Functionalization of MXenes for Tribological Purposes—A Critical Review. *Adv. Colloid Interface Sci.* **2022**, *309*, 102792. [CrossRef] [PubMed]
28. Alhabeb, M.; Maleski, K.; Anasori, B.; Lelyukh, P.; Clark, L.; Sin, S.; Gogotsi, Y. Guidelines for Synthesis and Processing of Two-Dimensional Titanium Carbide ($Ti_3C_2T_x$ MXene). *Chem. Mater.* **2017**, *29*, 7633–7644. [CrossRef]
29. Naguib, M.; Presser, V.; Lane, N.; Tallman, D.; Gogotsi, Y.; Lu, J.; Hultman, L.; Barsoum, M.W. Synthesis of a New Nanocrystalline Titanium Aluminum Fluoride Phase by Reaction of Ti2AlC with Hydrofluoric Acid. *RSC Adv.* **2011**, *1*, 1493. [CrossRef]
30. Li, L.; Li, G.; Tan, L.; Zhang, Y.; Wu, B. Highly Efficiently Delaminated Single-Layered MXene Nanosheets with Large Lateral Size. *Langmuir* **2017**, *33*, 9000–9006. [CrossRef]
31. Wang, L.; Zhang, H.; Wang, B.; Shen, C.; Zhang, C.; Hu, Q.; Zhou, A.; Liu, B. Synthesis and Electrochemical Performance of Ti3C2Tx with Hydrothermal Process. *Electron. Mater. Lett.* **2016**, *12*, 702–710. [CrossRef]
32. Peng, C.; Wei, P.; Chen, X.; Zhang, Y.; Zhu, F.; Cao, Y.; Wang, H.; Yu, H.; Peng, F. A Hydrothermal Etching Route to Synthesis of 2D MXene (Ti3C2, Nb2C): Enhanced Exfoliation and Improved Adsorption Performance. *Ceram. Int.* **2018**, *44*, 18886–18893. [CrossRef]
33. Yang, S.; Zhang, P.; Wang, F.; Ricciardulli, A.G.; Lohe, M.R.; Blom, P.W.M.; Feng, X. Fluoride-Free Synthesis of Two-Dimensional Titanium Carbide (MXene) Using A Binary Aqueous System. *Angew. Chem.—Int. Ed.* **2018**, *57*, 15491–15495. [CrossRef]
34. Numan, A.; Rafique, S.; Khalid, M.; Zaharin, H.A.; Radwan, A.; Mokri, N.A.; Ching, O.P.; Walvekar, R. Microwave-Assisted Rapid MAX Phase Etching and Delamination: A Paradigm Shift in MXene Synthesis. *Mater. Chem. Phys.* **2022**, *288*, 126429. [CrossRef]
35. Gerard, O.; Numan, A.; Krishnan, S.; Khalid, M.; Subramaniam, R.; Kasi, R. A Review on the Recent Advances in Binder-Free Electrodes for Electrochemical Energy Storage Application. *J. Energy Storage* **2022**, *50*, 104283. [CrossRef]
36. Gao, F.; Lu, Q.; Komarneni, S. Fast Synthesis of Cerium Oxide Nanoparticles and Nanorods. *J. Nanosci. Nanotechnol.* **2006**, *6*, 3812–3819. [CrossRef] [PubMed]
37. Rosa, R.; Ponzoni, C.; Leonelli, C. Direct Energy Supply to the Reaction Mixture during Microwave-Assisted Hydrothermal and Combustion Synthesis of Inorganic Materials. *Inorganics* **2014**, *2*, 191–210. [CrossRef]
38. Nageswara Rao, B.; Ramesh Kumar, P.; Padmaraj, O.; Venkateswarlu, M.; Satyanarayana, N. Rapid Microwave Assisted Hydrothermal Synthesis of Porous α-Fe 2 O 3 Nanostructures as Stable and High Capacity Negative Electrode for Lithium and Sodium Ion Batteries. *RSC Adv.* **2015**, *5*, 34761–34768. [CrossRef]
39. Agusu, L.; Ahmad, L.O.; Anggara, D.; Alimin; Mitsudo, S.; Fujii, Y.; Kikuchi, H. Microwave Hydrothermal Synthesis of Reduced Graphene Oxide: Effects of Microwave Power and Irradiation Time. *J. Phys. Conf. Ser.* **2018**, *1011*, 012012. [CrossRef]
40. Kashinath, L. Microwave-Hydrothermal Synthesis of Copper Sulphide Nanorods Embedded on Graphene Sheets as an Efficient Electrocatalyst for Excellent Hydrogen Evolution Reaction. *Fuel* **2021**, *291*, 120143. [CrossRef]

41. Nagarajan, T.; Mohammad, K.; Nanthini, S.; Priyanka, J.; Rashmi, W. Microwave Synthesis of Molybdenum Disulfide Nanoparticles Using Response Surface Methodology for Tribological Application. *Nanomaterials* **2022**, *12*, 3369. [CrossRef]
42. Pan, X.; Shinde, N.M.; Lee, M.; Kim, D.; Kim, K.H.; Kang, M. Controlled Nanosheet Morphology of Titanium Carbide Ti3C2Tx MXene via Drying Methods and Its Electrochemical Analysis. *J. Solid State Electrochem.* **2020**, *24*, 675–686. [CrossRef]
43. Ghidiu, M.; Lukatskaya, M.R.; Zhao, M.-Q.; Gogotsi, Y.; Barsoum, M.W. Conductive Two-Dimensional Titanium Carbide 'Clay' with High Volumetric Capacitance. *Nature* **2014**, *516*, 78–81. [CrossRef]
44. Said, Z.; Sundar, L.S.; Tiwari, A.K.; Ali, H.M.; Sheikholeslami, M.; Bellos, E.; Babar, H. Recent Advances on the Fundamental Physical Phenomena behind Stability, Dynamic Motion, Thermophysical Properties, Heat Transport, Applications, and Challenges of Nanofluids. *Phys. Rep.* **2022**, *946*, 1–94. [CrossRef]
45. Kamarulzaman, M.K.; Hisham, S.; Kadirgama, K.; Ramasamy, D.; Samykano, M.; Said, Z.; Pandey, A.K. Improvement in Stability and Thermophysical Properties of CNC-MXene Nanolubricant for Tribology Application. *J. Mol. Liq.* **2023**, *381*, 121695. [CrossRef]
46. Mukherjee, S. Preparation and Stability of Nanofluids-A Review. *IOSR J. Mech. Civ. Eng.* **2013**, *9*, 63–69. [CrossRef]
47. Markandan, K.; Nagarajan, T.; Walvekar, R.; Chaudhary, V.; Khalid, M. Enhanced Tribological Behaviour of Hybrid MoS2@Ti3C2 MXene as an Effective Anti-Friction Additive in Gasoline Engine Oil. *Lubricants* **2023**, *11*, 47. [CrossRef]
48. Bao, Z.; Bing, N.; Zhu, X.; Xie, H.; Yu, W. Ti3C2Tx MXene Contained Nanofluids with High Thermal Conductivity, Super Colloidal Stability and Low Viscosity. *Chem. Eng. J.* **2021**, *406*, 126390. [CrossRef]
49. Nagarajan, T.; Khalid, M.; Sridewi, N.; Jagadish, P.; Shahabuddin, S.; Muthoosamy, K.; Walvekar, R. Tribological, Oxidation and Thermal Conductivity Studies of Microwave Synthesised Molybdenum Disulfide (MoS2) Nanoparticles as Nano-Additives in Diesel Based Engine Oil. *Sci. Rep.* **2022**, *12*, 14108. [CrossRef]
50. Guo, J.; Wu, P.; Zeng, C.; Wu, W.; Zhao, X.; Liu, G.; Zhou, F.; Liu, W. Fluoropolymer Grafted Ti3C2Tx MXene as an Efficient Lubricant Additive for Fluorine-Containing Lubricating Oil. *Tribol. Int.* **2022**, *170*, 107500. [CrossRef]
51. Liu, L.; Zhou, M.; Jin, L.; Li, L.; Mo, Y.; Su, G.; Li, X.; Zhu, H.; Tian, Y. Recent Advances in Friction and Lubrication of Graphene and Other 2D Materials: Mechanisms and Applications. *Friction* **2019**, *7*, 199–216. [CrossRef]
52. Suresha, B.; Hemanth, G.; Rakesh, A.; Adarsh, K.M. Tribological Behaviour of Pongamia Oil as Lubricant with and without Halloysite Nanotubes Using Four-Ball Tester. In Proceedings of the International Conference on Materials, Manufacturing and Machining 2019, Tamilnadu, India, 8–9 March 2019; p. 030011. [CrossRef]
53. Fan, W.; Zhu, X.; Ke, F.; Chen, Y.; Dong, K.; Ji, J.; Chen, B.; Tongay, S.; Ager, J.W.; Liu, K.; et al. Vibrational Spectrum Renormalisation by Enforced Coupling across the van Der Waals Gap between MoS2 and WS2 Monolayers. *Phys. Rev. B* **2015**, *92*, 24408. [CrossRef]
54. Rosenkranz, A.; Grützmacher, P.G.; Espinoza, R.; Fuenzalida, V.M.; Blanco, E.; Escalona, N.; Gracia, F.J.; Villarroel, R.; Guo, L.; Kang, R.; et al. Multi-Layer Ti3C2Tx-Nanoparticles (MXenes) as Solid Lubricants—Role of Surface Terminations and Intercalated Water. *Appl. Surf. Sci.* **2019**, *494*, 13–21. [CrossRef]
55. Zhang, X.; Guo, Y.; Li, Y.; Liu, Y.; Dong, S. Preparation and Tribological Properties of Potassium Titanate-Ti3C2Tx Nanocomposites as Additives in Base Oil. *Chin. Chem. Lett.* **2019**, *30*, 502–504. [CrossRef]
56. Jin, W.; Jiang, L.; Han, L.; Huang, H.; Zhang, J.; Guo, M.; Gu, Y.; Zhi, F.; Chen, Z.; Yang, G. Investigation of Thermal Conductivity Enhancement of Water-Based Graphene and Graphene/MXene Nanofluids. *J. Mol. Liq.* **2022**, *367*, 120455. [CrossRef]
57. Walvekar, R.; Faris, I.A.; Khalid, M. Thermal Conductivity of Carbon Nanotube Nanofluid-Experimental and Theoretical Study. *Heat Transf.—Asian Res.* **2012**, *41*, 145–163. [CrossRef]
58. Baby, T.T.; Ramaprabhu, S. Investigation of Thermal and Electrical Conductivity of Graphene Based Nanofluids. *J. Appl. Phys.* **2010**, *108*, 124308. [CrossRef]
59. Aslfattahi, N.; Samylingam, L.; Abdelrazik, A.S.; Arifutzzaman, A.; Saidur, R. MXene Based New Class of Silicone Oil Nanofluids for the Performance Improvement of Concentrated Photovoltaic Thermal Collector. *Sol. Energy Mater. Sol. Cells* **2020**, *211*, 110526. [CrossRef]
60. Qing, S.H.; Rashmi, W.; Khalid, M.; Gupta, T.C.S.M.; Nabipoor, M.; Hajibeigy, M.T. Thermal Conductivity and Electrical Properties of Hybrid SiO 2 -Graphene Naphthenic Mineral Oil Nanofluid as Potential Transformer Oil. *Mater. Res. Express* **2017**, *4*, 015504. [CrossRef]
61. Yiamsawas, T.; Dalkilic, A.S.; Mahian, O.; Wongwises, S. Measurement and Correlation of the Viscosity of Water-Based Al2O3 and TiO2 Nanofluids in High Temperatures and Comparisons with Literature Reports. *J. Dispers. Sci. Technol.* **2013**, *34*, 1697–1703. [CrossRef]
62. Malekzadeh, A.; Pouranfard, A.R.; Hatami, N.; Kazemnejad Banari, A.; Rahimi, M.R. Experimental Investigations on the Viscosity of Magnetic Nanofluids under the Influence of Temperature, Volume Fractions of Nanoparticles and External Magnetic Field. *J. Appl. Fluid Mech.* **2016**, *9*, 693–697. [CrossRef]
63. Apmann, K.; Fulmer, R.; Soto, A.; Vafaei, S. Thermal Conductivity and Viscosity: Review and Optimisation of Effects of Nanoparticles. *Materials* **2021**, *14*, 1291. [CrossRef] [PubMed]
64. Chen, J.; Zhao, W. Simple Method for Preparing Nanometer Thick Ti3C2TX Sheets towards Highly Efficient Lubrication and Wear Resistance. *Tribol. Int.* **2021**, *153*, 106598. [CrossRef]
65. Nguyen, H.T.; Chung, K.-H. Assessment of Tribological Properties of Ti3C2 as a Water-Based Lubricant Additive. *Materials* **2020**, *13*, 5545. [CrossRef]
66. Liu, Y. Synthesis and Tribological Property of Ti3C2TX Nanosheets. *J. Mater. Sci.* **2016**, *52*, 2200–2209. [CrossRef]

67. Xue, M.; Wang, Z.; Yuan, F.; Zhang, X.; Wei, W.; Tang, H.; Li, C. Preparation of TiO2/Ti3C2Tx Hybrid Nanocomposites and Their Tribological Properties as Base Oil Lubricant Additives. *RSC Adv.* **2017**, *7*, 4312–4319. [CrossRef]
68. Zhang, X.; Xue, M.; Yang, X.; Wang, Z.; Luo, G.; Huang, Z.; Sui, X.; Li, C. Preparation and Tribological Properties of Ti3C2(OH)2 Nanosheets as Additives in Base Oil. *RSC Adv.* **2015**, *5*, 2762–2767. [CrossRef]
69. Yang, J.; Chen, B.; Song, H.; Tang, H.; Li, C. Synthesis, Characterization, and Tribological Properties of Two-Dimensional Ti3C2. *Cryst. Res. Technol.* **2014**, *49*, 926–932. [CrossRef]
70. Feng, Q.; Deng, F.; Li, K.; Dou, M.; Zou, S.; Huang, F. Enhancing the Tribological Performance of Ti3C2 MXene Modified with Tetradecylphosphonic Acid. *Colloids Surf. A Physicochem. Eng. Asp.* **2021**, *625*, 126903. [CrossRef]
71. Gao, J.; Du, C.-F.; Zhang, T.; Zhang, X.; Ye, Q.; Liu, S.; Liu, W. Dialkyl Dithiophosphate-Functionalized Ti3C2Tx MXene Nanosheets as Effective Lubricant Additives for Antiwear and Friction Reduction. *ACS Appl. Nano Mater.* **2021**, *4*, 11080–11087. [CrossRef]
72. Zhang, F.X.; Su, X.; Tang, G.G.; Xu, J. Construction and Tribological Behaviors of MXenes/MoS2 Heterojunction with 2D/2D Structure in Liquid Paraffin. *Chalcogenide Lett.* **2021**, *18*, 225–235. [CrossRef]
73. Feng, P.; Ren, Y.; Li, Y.; He, J.; Zhao, Z.; Ma, X.; Fan, X.; Zhu, M. Synergistic Lubrication of Few-Layer Ti3C2Tx/MoS2 Heterojunction as a Lubricant Additive. *Friction* **2022**, *10*, 2018–2032. [CrossRef]
74. Zhou, C.; Li, Z.; Liu, S.; Ma, L.; Zhan, T.; Wang, J. Synthesis of MXene-Based Self-Dispersing Additives for Enhanced Tribological Properties. *Tribol. Lett.* **2022**, *70*, 63. [CrossRef]
75. Jazaa, Y.; Lan, T.; Padalkar, S.; Sundararajan, S. The Effect of Agglomeration Reduction on the Tribological Behavior of WS2 and MoS2 Nanoparticle Additives in the Boundary Lubrication Regime. *Lubricants* **2018**, *6*, 106. [CrossRef]
76. Guo, Y.B.; Zhang, S.W. The Tribological Properties of Multi-Layered Graphene as Additives of PAO2 Oil in Steel-Steel Contacts. *Lubricants* **2016**, *4*, 30. [CrossRef]
77. Azman, S.S.N.; Zulkifli, N.W.M.; Masjuki, H.; Gulzar, M.; Zahid, R. Study of Tribological Properties of Lubricating Oil Blend Added with Graphene Nanoplatelets. *J. Mater. Res.* **2016**, *31*, 1932–1938. [CrossRef]
78. Cai, Z.B.; Zhao, L.; Zhang, X.; Yue, W.; Zhu, M.H. Combined Effect of Textured Patterns and Graphene Flake Additives on Tribological Behavior under Boundary Lubrication. *PLoS ONE* **2016**, *11*, e0152143. [CrossRef] [PubMed]
79. Zheng, D.; Cai, Z.B.; Shen, M.X.; Li, Z.Y.; Zhu, M.H. Investigation of the Tribology Behaviour of the Graphene Nanosheets as Oil Additives on Textured Alloy Cast Iron Surface. *Appl. Surf. Sci.* **2016**, *387*, 66–75. [CrossRef]
80. Kiu, S.S.K.; Yusup, S.; Soon, C.V.; Arpin, T.; Samion, S.; Kamil, R.N.M. Tribological Investigation of Graphene as Lubricant Additive in Vegetable Oil. *J. Phys. Sci.* **2017**, *28*, 257–267. [CrossRef]
81. Li, X.; Liu, Q.; Dong, G. Self-Assembly Membrane on Textured Surface for Enhancing Lubricity of Graphene Oxide Nano-Additive. *Appl. Surf. Sci.* **2020**, *505*, 144572. [CrossRef]
82. Wu, P.; Chen, X.; Zhang, C.; Luo, J. Synergistic Tribological Behaviors of Graphene Oxide and Nanodiamond as Lubricating Additives in Water. *Tribol. Int.* **2019**, *132*, 177–184. [CrossRef]
83. Yang, J.; Xia, Y.; Song, H.; Chen, B.; Zhang, Z. Synthesis of the Liquid-like Graphene with Excellent Tribological Properties. *Tribol. Int.* **2017**, *105*, 118–124. [CrossRef]
84. Gao, T.; Li, C.; Zhang, Y.; Yang, M.; Jia, D.; Jin, T.; Hou, Y.; Li, R. Dispersing Mechanism and Tribological Performance of Vegetable Oil-Based CNT Nanofluids with Different Surfactants. *Tribol. Int.* **2019**, *131*, 51–63. [CrossRef]